Chromatin remodeler *Arid1a* regulates subplate neuron identity and wiring of cortical connectivity

Daniel Z. Doyle[a,b,c], Mandy M. Lam[a,b], Adel Qalieh[a,b], Yaman Qalieh[a,b], Alice Sorel[a,b], Owen H. Funk[a,b], and Kenneth Y. Kwan[a,b,c,1]

[a]Michigan Neuroscience Institute, University of Michigan, Ann Arbor, MI 48109; [b]Department of Human Genetics, University of Michigan, Ann Arbor, MI 48109; and [c]Neuroscience Graduate Program, University of Michigan, Ann Arbor, MI 48109

Edited by Jeremy Nathans, Johns Hopkins University School of Medicine, Baltimore, MD, and approved April 15, 2021 (received for review January 14, 2021)

Loss-of-function mutations in chromatin remodeler gene *ARID1A* are a cause of Coffin-Siris syndrome, a developmental disorder characterized by dysgenesis of corpus callosum. Here, we characterize *Arid1a* function during cortical development and find unexpectedly selective roles for *Arid1a* in subplate neurons (SPNs). SPNs, strategically positioned at the interface of cortical gray and white matter, orchestrate multiple developmental processes indispensable for neural circuit wiring. We find that pancortical deletion of *Arid1a* leads to extensive mistargeting of intracortical axons and agenesis of corpus callosum. Sparse *Arid1a* deletion, however, does not autonomously misroute callosal axons, implicating noncell-autonomous *Arid1a* functions in axon guidance. Supporting this possibility, the ascending axons of thalamocortical neurons, which are not autonomously affected by cortical *Arid1a* deletion, are also disrupted in their pathfinding into cortex and innervation of whisker barrels. Coincident with these miswiring phenotypes, which are reminiscent of subplate ablation, we unbiasedly find a selective loss of SPN gene expression following *Arid1a* deletion. In addition, multiple characteristics of SPNs crucial to their wiring functions, including subplate organization, subplate axon-thalamocortical axon cofasciculation ("handshake"), and extracellular matrix, are severely disrupted. To empirically test *Arid1a* sufficiency in subplate, we generate a cortical plate deletion of *Arid1a* that spares SPNs. In this model, subplate *Arid1a* expression is sufficient for subplate organization, subplate axon-thalamocortical axon cofasciculation, and subplate extracellular matrix. Consistent with these wiring functions, subplate *Arid1a* sufficiently enables normal callosum formation, thalamocortical axon targeting, and whisker barrel development. Thus, *Arid1a* is a multifunctional regulator of subplate-dependent guidance mechanisms essential to cortical circuit wiring.

cerebral cortex | development | chromatin regulation | axon pathfinding | neural circuits

The subplate (SP) is a transient layer of the fetal cerebral cortex essential to the developmental wiring of cortical circuits (1–11). During neurogenesis, cortical neural progenitor cells (NPCs) generate excitatory neurons following an orderly temporal progression, successively giving rise to SP neurons (SPNs), then deep-layer neurons, then upper-layer neurons (12). As the first neurons generated from embryonic cortex, SPNs establish emerging axon tracts and form the earliest synapses (1–4, 13–16). Importantly, SPNs, which are strategically positioned at the interface between postmigratory neurons and developing white matter (WM), serve noncell-autonomous wiring functions in cortical circuit formation. Experimental SP ablation during fetal development causes thalamocortical axon (TCA) misrouting (17–19) and disrupts sensory map formation (20, 21), and perturbed SP function has been hypothesized to contribute to circuit defects in disorders of brain development (22–24). Mechanistically, SPNs noncell-autonomously mediate circuit wiring in part by extending the earliest descending axons, which interact with ascending TCAs during pathfinding (as posited by the "handshake hypothesis") (25, 26) and contribute to their crossing of the pallial-subpallial boundary (PSB) (27, 28). SPNs also secrete extracellular matrix components that support axon guidance (4, 29) and are required for early oscillatory activity (8, 13). In postnatal ages, some SPNs undergo programmed cell death (30), thereby serving a transient role in cortical development.

Despite the central position of SPNs in orchestrating cortical connectivities, the molecular determinants of SP wiring functions remain largely elusive. Previous studies have focused on genes selectively expressed in SPNs (23, 31) and illuminated the genetic bases of SPN specification, migration, and axon development (32–38). The axon misrouting phenotypes of SP ablation (17–19), however, are not broadly recapitulated in these genetic mutants. The mechanisms underpinning SP guidance functions have remained largely mysterious. Here, by cell type-specific dissection of gene function, we identify *Arid1a* as a key regulator of multiple SP-dependent axon guidance mechanisms indispensable for cortical circuit wiring.

Arid1a (*Baf250a*) encodes a subunit of the Brg/Brahma-associated factors (BAF, or mammalian SWI/SNF) ATP-dependent chromatin remodeling complex that mobilizes nucleosomes along DNA, thereby mediating processes such as transcription and DNA repair. Human genetic studies have identified *ARID1A* loss-of-function mutations in intellectual disability, autism spectrum disorder, and Coffin-Siris syndrome, a developmental disorder characterized by callosal dysgenesis (39). BAF is broadly present in cells and organs (40), and cell type-dependent subunit compositions of the complex play diverse roles in embryonic stem cells, NPCs, and neurons (41). *Arid1a*, however, is not known to incorporate into BAF cell type

Significance

The cognitive, perceptive, and motor capabilities of the mammalian cerebral cortex depend on assembly of circuit connectivity during development. Subplate neurons, strategically located at the junction of gray and white matter, orchestrate the wiring of cortical circuits. Using a genetic approach to study gene necessity and sufficiency in subplate neurons, we uncover an essential role for chromatin remodeler *Arid1a* in subplate neuron gene expression and axon guidance functions. Cortical deletion of *Arid1a* disrupts subplate-dependent formation of corpus callosum, targeting of thalamocortical axons, and development of sensory maps. Together, our study identifies *Arid1a* as a central regulator of subplate-dependent axon pathfinding, establishes subplate function as essential to callosum development, and highlights noncell-autonomous mechanisms in neural circuit formation and disorders thereof.

Author contributions: D.Z.D. and K.Y.K. designed research; D.Z.D., M.M.L., and A.S. performed research; D.Z.D., A.Q., Y.Q., O.H.F., and K.Y.K. analyzed data; and D.Z.D. and K.Y.K. wrote the paper.

The authors declare no competing interest.

This article is a PNAS Direct Submission.

[1]To whom correspondence may be addressed. Email: kykwan@umich.edu.

This article contains supporting information online at https://www.pnas.org/lookup/suppl/doi:10.1073/pnas.2100686118/-/DCSupplemental.

Published May 19, 2021.

specifically, and its potential context-dependent roles remain underexplored.

Here, we leverage a conditional allele to cell type specifically manipulate *Arid1a* function. We find that pancortical *Arid1a* deletion leads to extensive intracortical axon mistargeting and corpus callosum (CC) agenesis. Surprisingly, unlike pancortical deletion, sparse *Arid1a* deletion does not cell-autonomously misroute callosal axons, suggesting axon mistargeting to be a noncell-autonomous consequence of pancortical *Arid1a* deletion. Supporting this possibility, the axons of thalamocortical neurons, which are not autonomously affected by cortical *Arid1a* deletion, are also strikingly disrupted in their pathfinding into cortex and innervation of whisker barrels. *Arid1a* thus plays essential, noncell-autonomous roles in development of cortical axon tracts. By transcriptome analysis, we unbiasedly find a selective loss of SPN gene expression following *Arid1a* deletion, thus identifying SP as a potential substrate of *Arid1a* phenotypes. Consistent with this, *Arid1a* axon misrouting defects are reminiscent of SP ablation (17–19). Furthermore, SPN characteristics crucial to their circuit wiring functions, including SP organization and extracellular

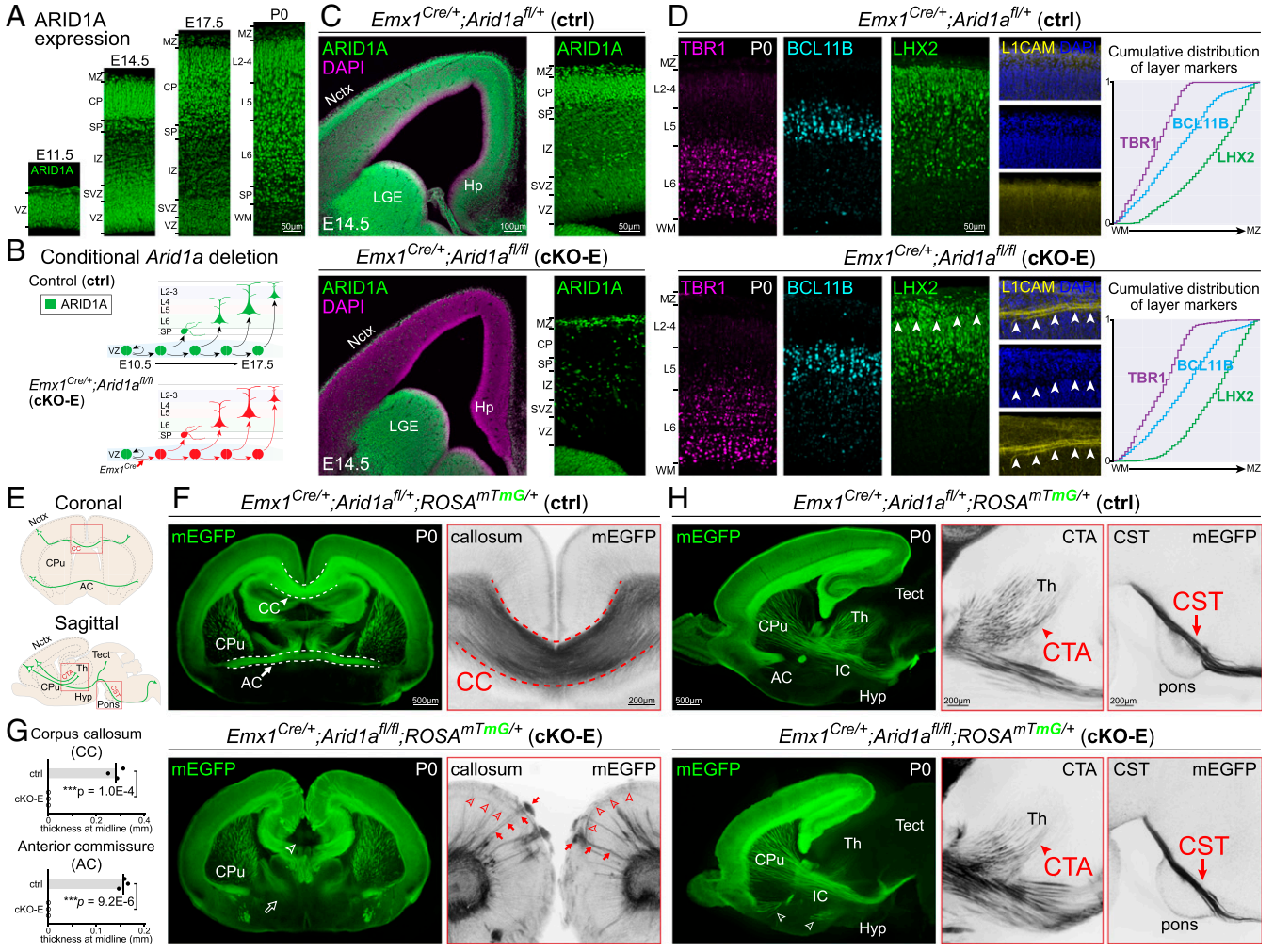

Fig. 1. Tract-dependent misrouting of cortical axons following conditional *Arid1a* deletion. (*A*) ARID1A (green) immunostaining on coronal E11.5, E14.5, E17.5, and P0 brain sections revealed widespread ARID1A expression during cortical development. (*B*) Schematic illustration of conditional *Arid1a* deletion using $Emx1^{Cre}$, which mediates recombination in cortical NPCs at E10.5, near the onset of neurogenesis. (*C*) ARID1A (green) and DAPI (magenta) staining of coronal E14.5 $Emx1^{Cre/+};Arid1a^{fl/fl}$ (cKO-E) brain sections revealed loss of ARID1A from VZ and subventricular zone NPCs and CP neurons. ARID1A expression was unaffected in the ventral forebrain. (*D*) Layer marker immunostaining on coronal P0 brain sections. TBR1+ (L6, magenta), BCL11B+ (L5, cyan), and LHX2+ (L2 to 5, green) neurons were correctly ordered in cKO-E. Cumulative distribution of layer marker-expressing neurons from WM to marginal zone (MZ) revealed no disruption in cortical lamination in cKO-E ($n = 3$ animals). In all analyzed cKO-E brains (3/3 animals), but no littermate ctrl brains (0/3 animals), a stereotyped gap (arrowheads) in LHX2 and DAPI (blue) staining was present in upper cortical layers. This gap contained misrouted L1CAM+ (yellow) axons. (*E*) Schematic illustration of cortical axon tracts on coronal and sagittal brain sections. (*F*) Coronal sections of P0 brains. mEGFP (green) was expressed Cre dependently from $ROSA^{mTmG}$, enabling visualization of cortical axons. Callosal agenesis (open arrowhead) was observed in cKO-E (3/3 animals). AC also failed to form (open arrow). cKO-E cortex was characterized by widespread axon misrouting (3/3 animals), including radially directed axons extending to the pia (red arrows) and tangentially directed axons traveling across the upper layers (red arrowheads). (*G*) Quantification of callosum and AC thickness at midline (data are mean, two-tailed unpaired *t* test, $n = 3$ animals). (*H*) Sagittal sections of P0 brains. In cKO-E, corticofugal axons innervated internal capsule. Corticothalamic axons (CTA, red arrowheads), corticotectal axons, and corticospinal tract (CST) axons (red arrows) were qualitatively reduced but followed normal trajectories without misrouting defects in cKO-E. AC axons were misrouted to the hypothalamus (Hyp, open arrowheads). VZ, ventricular zone; SVZ, subventricular zone; PP, preplate; IZ, intermediate zone; SP, subplate; CP, cortical plate; MZ, marginal zone; Ln, layer n; WM, white matter; Nctx, neocortex; Hp, hippocampus; LGE, lateral ganglionic eminence; CC, corpus callosum; AC, anterior commissure; CPu, caudate putamen; CTA, corticothalamic axons; CST, corticospinal tract; Th, thalamus; Tect, tectum; Hyp, hypothalamus.

matrix, are disrupted following *Arid1a* deletion. Importantly, descending SP axons are severely attenuated, abrogating their cofasciculation with ascending TCAs. This "handshake" interaction is essential to TCA pathfinding and whisker barrel formation (25, 26), both of which are disrupted by *Arid1a* deletion. Thus, we find a necessity for *Arid1a* in orchestrating distinct aspects of SP wiring functions. To empirically test *Arid1a* sufficiency in SPNs, we use a genetic approach for cortical plate (CP) deletion of *Arid1a* that spares SPNs. In this model, *Arid1a* expression in SPNs is sufficient to support SP organization, SP axon "handshake" with TCAs, and SP extracellular matrix. Consistent with these wiring functions, SP *Arid1a* expression sufficiently enables normal TCA targeting, whisker barrel development, and callosum formation. Together, our study identifies *Arid1a* as a central regulator of SP-dependent axon pathfinding, unequivocally establishes SP function as essential to callosal development, and highlights noncell-autonomous mechanisms in circuit development and disorders thereof.

Results

Mistargeting of Intracortical, but Not Corticofugal, Axons following *Arid1a* Deletion from NPCs. We analyzed ARID1A protein in developing mouse cortex by immunostaining and found broad ARID1A expression in ventricular zone (VZ) and subventricular zone NPCs and CP neurons from embryonic day (E)11.5 to postnatal day (P)0 (Fig. 1*A*). ARID1A completely colocalized with DAPI DNA staining at E14.5 (*SI Appendix*, Fig. S1*A*), which is consistent with ubiquitous ARID1A expression during cortical development. Constitutive *Arid1a* deletion leads to lethality on E6.5 in mice (42). We therefore leveraged a conditional allele (42) to investigate *Arid1a* function during brain development.

To delete *Arid1a* from developing cortex, we used $Emx1^{Cre}$, which expresses Cre recombinase in cortical NPCs starting at ~E10.5, near cortical neurogenesis onset (Fig. 1*B*) (43). *Arid1a* deletion was validated in $Emx1^{Cre/+}$;$Arid1a^{fl/fl}$ (cKO-E) by ARID1A immunostaining, which revealed ARID1A loss from cortical NPCs and neurons of the *Emx1* lineage (Fig. 1*C*). cKO-E mice were born at Mendelian ratio, had typical lifespans, and were fertile. At P0, cKO-E cortical area was not significantly different from control (ctrl) littermates (*SI Appendix*, Fig. S1 *B* and *C*).

To assess neocortical layers, we analyzed laminar markers at P0 (Fig. 1*D*). We found largely normal cortical lamination in cKO-E; TBR1+ layer (L)6, BCL11B+ (CTIP2+) L5, and LHX2+ L2 to 5 neurons were properly ordered and not robustly different from ctrl based on marker quantification (*SI Appendix*, Fig. S1*D*) and cumulative distribution of layer markers (Fig. 1*D*). However, a stereotyped gap in marker and DAPI staining was present in upper layers (L2 to 4) of all analyzed cKO-E brains (arrowheads, Fig. 1*D*, 3/3 animals) but absent from ctrls (0/3 animals). This gap was characterized by aberrant L1CAM-immunostained axons (arrowheads, Fig. 1*D*), suggesting the presence of misrouted axons in cKO-E.

We examined potential changes in axonal projections using Cre-dependent reporter $ROSA^{mTmG}$. Following $Emx1^{Cre}$ recombination, membrane EGFP (mEGFP) was expressed from $ROSA^{mTmG}$ in all cortical excitatory neurons, enabling visualization of their axon projections (schematized in Fig. 1*E*). In P0 ctrl, mEGFP expression revealed intracortical axon tracts (CC and anterior commissure [AC]) (Fig. 1*F*). In cKO-E, we found callosal agenesis and widespread axon misrouting, including radially directed axons toward the pia (arrows) and tangentially directed axons through upper layers (arrowheads, Fig. 1*F*). These misrouting phenotypes were confirmed by L1CAM immunostaining (*SI Appendix*, Fig. S1*E*). AC axons were also mistargeted and unable to cross the midline (Fig. 1*F* and *SI Appendix*, Fig. S1*F*). Analysis of callosal and commissural thickness revealed loss of these tracts at the midline in cKO-E (Fig. 1*G*). Axon misrouting was also present in the hippocampus and accompanied hippocampal hypoplasia and disorganization (*SI Appendix*, Fig. S1*G*).

In contrast to intracortical axons, corticofugal tracts (corticothalamic, corticotectal, and corticospinal) were not characterized by gross misrouting deficits in cKO-E (Fig. 1*H*). These tracts were qualitatively reduced in strength but followed normal trajectories out of cortex and through internal capsule, and innervated their targets in dorsal thalamus, tectum, and medulla. Together, our axonal analyses revealed widespread mistargeting of intracortical but not corticofugal axon tracts following *Arid1a* deletion, implicating a tract-dependent role for *Arid1a*.

Noncell-Autonomous Misrouting of TCAs following *Arid1a* Deletion. We next analyzed TCAs (schematized in Fig. 2*A*). In cKO-E, thalamocortical neurons were not autonomously affected by cortical *Arid1a* deletion; however, their axonal target, the cortex, was broadly affected by $Emx1^{Cre}$. We used cytochrome oxidase (CO) histochemistry on flattened P7 cortex to visualize whisker barrels, a major target of TCAs. In P7 ctrl, CO staining revealed discrete, stereotyped, and organized whisker barrels in primary somatosensory cortex (Fig. 2*B* and *SI Appendix*, Fig. S2*A*). In cKO-E, barrel formation was severely disrupted; many barrels were missing and remaining barrels were distorted and disorganized. These TCA targeting defects were confirmed by immunostaining for TCA marker NTNG1 (Netrin G1) (Fig. 2*B*). In addition, analysis of P0 cKO-E revealed that NTNG1+ axons deviated from their normal trajectory in WM (arrowheads, Fig. 2*C*) and became markedly misrouted, including into tangential bundles through upper cortical layers and toward midline. Interestingly, TCAs largely did not contribute to radially directed aberrant axons in cKO-E, which were revealed by panaxonal marker L1CAM (arrows, Fig. 2*C*) and $ROSA^{mTmG}$ expression (arrows, *SI Appendix*, Fig. S2*B*).

TCAs normally follow a precise developmental path. In ctrl E15.5 cortex, NTNG1+ TCAs had crossed the PSB into pallium and reached SP. Consistent with the "waiting period" (4, 44), TCAs at this age paused their ingrowth within SP and had not entered CP (Fig. 2*D*). Remarkably, in cKO-E, NTNG1+ axons prematurely invaded CP as aberrant bundles (arrowheads, Fig. 2*D*). By E16.5, we found an abundance of TCAs prematurely invading CP (Fig. 2*E*). This bypassing of the waiting period by TCAs is reminiscent of SP ablation (17, 18). In addition, cKO-E NTNG1+ axons did not cross the PSB along the normal path. Instead, they formed an abnormal bundle running parallel to the PSB (arrow, Fig. 2*D* and *SI Appendix*, Fig. S2*C*) and ultimately entered the pallium via a narrow medial trajectory. Impaired PSB crossing of TCAs is also a consequence of disrupted SP function (27, 28). Together, TCA phenotypes following cortex-specific *Arid1a* deletion in cKO-E revealed noncell-autonomous *Arid1a* functions in axon guidance.

Correct Callosal Axon Targeting following Sparse Deletion of *Arid1a*. To determine whether intracortical axon misrouting in cKO-E also resulted from disrupted noncell-autonomous *Arid1a* function, we sought to sparsely delete *Arid1a* by in utero electroporation (IUE). We generated a self-excising, self-reporting *Cre* construct (CAG-sxiCre-EGFP) that expresses Cre, and upon Cre recombination, simultaneously excises *Cre* and turns on EGFP expression (*SI Appendix*, Fig. S3*A*). The sxiCre construct was transfected into embryonic cortex by IUE (37) at E14.5 to target NPCs during the genesis of upper-layer neurons, which form the majority of callosal axons. Transfected brains were analyzed at P0. To directly compare the effects of sparse versus widespread loss of *Arid1a*, we used ctrl, cKO-E (pancortical), and $Arid1a^{fl/fl}$ (sparse by Cre transfection) littermates for IUE. In $Arid1a^{fl/fl}$, ARID1A immunostaining revealed 97.67% deletion efficacy by sxiCre in EGFP+ cells (*SI Appendix*, Fig. S3*B*). In P0 ctrl, electroporated neurons migrated to upper cortical layers and projected EGFP+ axons across the CC

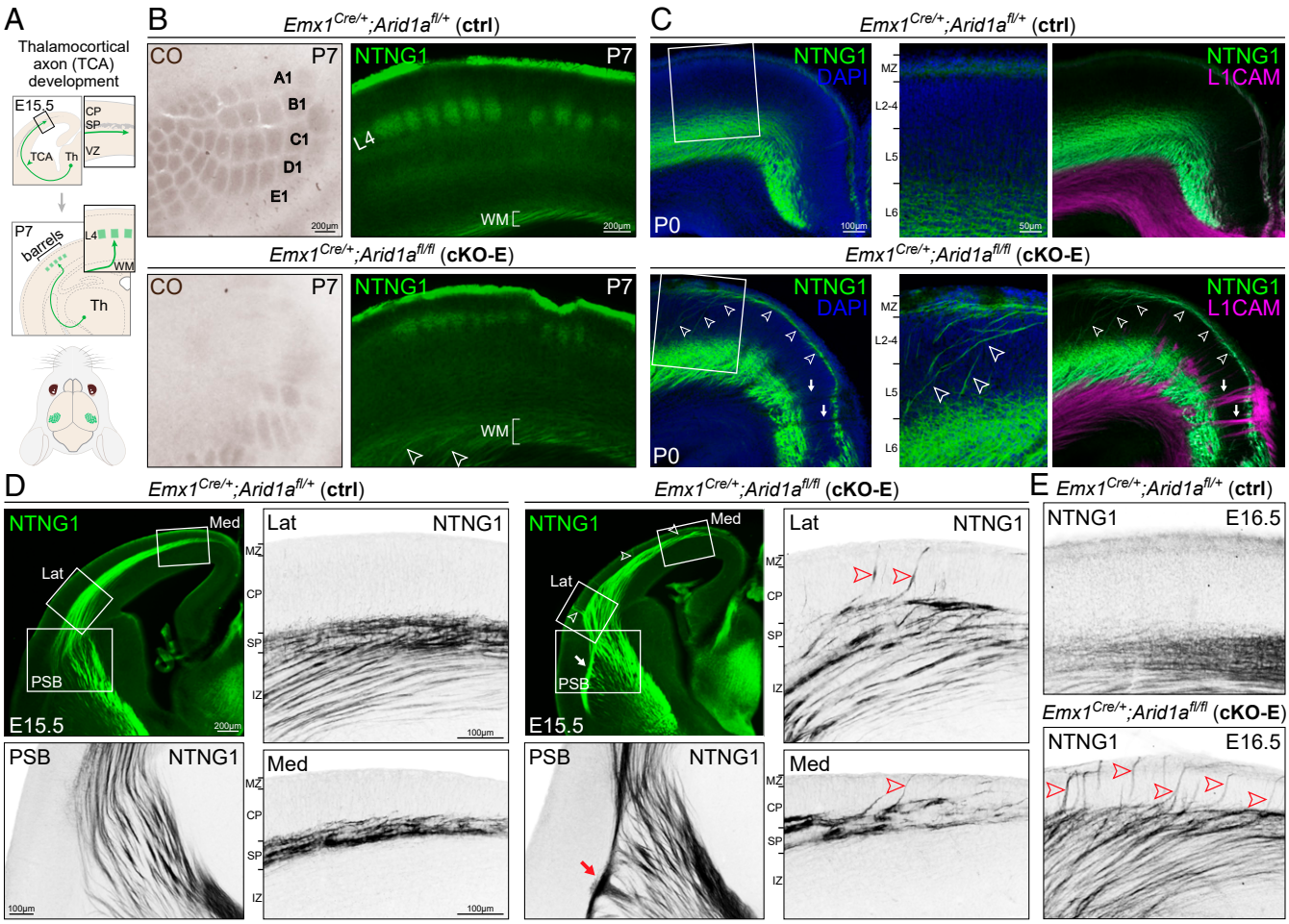

Fig. 2. Noncell-autonomous disruption of TCA pathfinding following *Arid1a* deletion. (*A*) Schematic illustration of TCA development. (*B*) Whisker barrels in P7 primary somatosensory cortex were visualized by CO staining (brown) on flattened cortices and NTNG1 immunostaining (green) on coronal sections. In cKO-E, barrel formation was severely disrupted (4/4 animals). Many barrels were missing, and the remaining barrels were distorted or disorganized. In cKO-E, NTNG1+ TCAs were defasciculated in cortical WM (open arrowheads). (*C*) NTNG1 immunostaining (green) on coronal P0 sections. In ctrl, NTNG1+ TCAs were present in WM, L6, and marginal zone (MZ). In cKO-E, NTNG1+ TCAs were markedly misrouted, extending dorsally from WM through the cortical layers (arrowheads). These aberrant axons then traveled tangentially across the upper layers and toward the midline. NTNG1+ TCAs did not contribute to radially directed axon bundles labeled by L1CAM (magenta, arrows) in cKO-E. (*D*) Analysis of TCA development at E15.5. In ctrl, NTNG1+ TCAs ascended across the PSB and paused within SP during the embryonic "waiting period." In cKO-E, NTNG1+ TCAs did not cross the PSB along the normal trajectory (3/3 animals). They formed an aberrant bundle parallel to the PSB (red arrow) and entered the cortex via a narrow medial path. Notably, NTNG1+ TCAs prematurely invaded CP in the lateral (Lat) and medial (Med) cortex (red arrowheads) (3/3 animals). (*E*) Analysis of E16.5 cortex revealed an abundance of NTNG1+ TCAs prematurely invading CP in cKO-E (red arrowheads).

(Fig. 3 *A*–*C*). Following broad, genetic deletion of *Arid1a* in cKO-E, electroporated neurons migrated to upper layers, although their positioning was qualitatively less organized and potentially affected by misrouted axons (Fig. 1*D*). In cKO-E, axons originating from transfected neurons failed to project into CC (Fig. 3 *D*–*F*) and contributed to aberrant radially directed bundles (*SI Appendix*, Fig. S3*C*). Following sparse *Arid1a* deletion by sxiCre IUE in *Arid1a*$^{fl/fl}$, electroporated neurons migrated to upper layers without deficit (Fig. 3 *G* and *H*). Remarkably, despite ARID1A loss, these neurons abundantly extended EGFP+ axons into CC and correctly targeted contralateral cortex in a manner indistinguishable from ctrl (Fig. 3*I*). Together, our results provided strong support that the callosal and TCA pathfinding defects in cKO-E were noncell-autonomous consequences of broad cortical *Arid1a* deletion.

Selective Disruption of SPN Gene Expression following *Arid1a* Deletion. To gain mechanistic insights into the axon guidance roles of *Arid1a*, we explored its molecular functions. As a chromatin remodeler, ARID1A mediates transcriptional regulation (45, 46). We thus analyzed the transcriptomes of cKO-E and littermate ctrl cortices at E15.5, a developmental stage when cortical axons and TCAs undergo pathfinding (47). We generated libraries for unique molecular identifier (UMI) RNA sequencing (RNA-seq) (48–50) from E15.5 cKO-E and littermate ctrl cortices (ctrl: $n = 6$, cKO-E: $n = 6$ animals, *SI Appendix*, Fig. S4*A*). Differential gene expression was analyzed using edgeR (51), which revealed significant differential expression of 103 genes in cKO-E compared to ctrl with a stringent false discovery rate of <0.01 (Fig. 4*A*). Gene expression changes were validated by droplet digital (dd)RT-PCR for two down-regulated genes (*Tle4* and *Zfpm2*) and two genes without significant changes (*Lhx2* and *Tbr1*) and by TLE4 immunostaining (*SI Appendix*, Fig. S4*B*).

Arid1a has been shown to increase or maintain transcriptional activity (46), which is consistent with our finding that a majority of differentially expressed genes were down-regulated in cKO-E (91/103). To determine whether axon defects in cKO-E may be associated with reduced expression of axon extension or guidance genes, we intersected the 91 down-regulated genes with 253

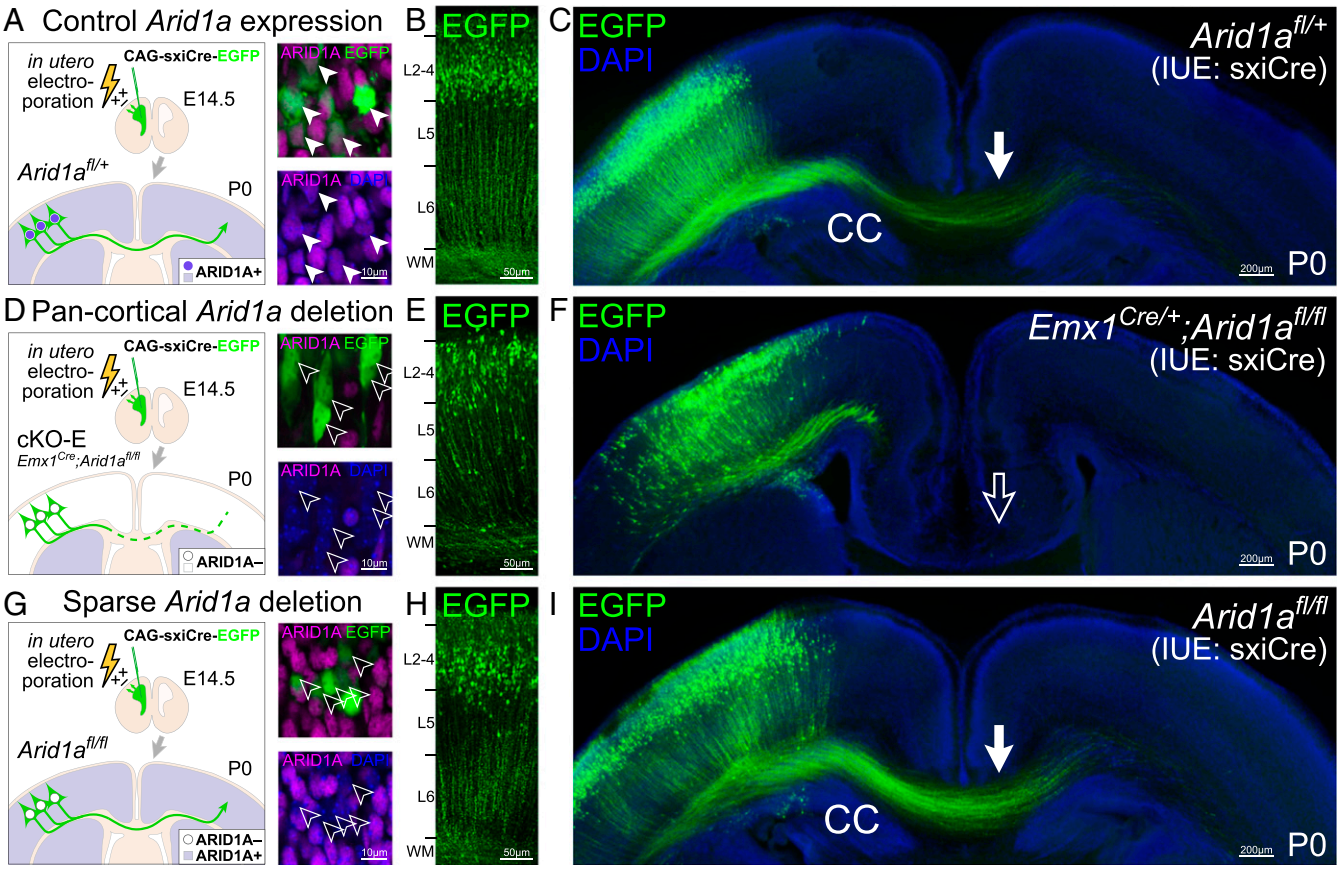

Fig. 3. Correct callosal axon targeting following sparse deletion of *Arid1a*. A self-excising Cre expression EGFP reporter construct (CAG-sxiCre-EGFP or sxiCre) was transfected into dorsal cortical NPCs of *Arid1a*$^{fl/+}$ (ctrl, *A–C*), *Emx1*$^{Cre/+}$;*Arid1a*$^{fl/fl}$ (cKO-E, *D–F*), and *Arid1a*$^{fl/fl}$ (without genetic Cre, *G–I*) using IUE at E14.5. At P0, ARID1A expression (magenta) was analyzed in EGFP+ transfected cells by immunostaining. ARID1A was present in transfected ctrl EGFP+ cells (solid arrowheads, *A*) but lost following pancortical genetic *Arid1a* deletion (cKO-E, open arrowheads, *D*) or sparse *Arid1a* deletion (*Arid1a*$^{fl/fl}$, open arrowheads, *G*). EGFP+ cells migrated to upper cortical layers in each condition (*B*, *E*, and *H*). EGFP+ axons innervated CC in ctrl (solid arrow, *C*) but failed to do so following broad *Arid1a* deletion in cKO-E (open arrow, *F*). Remarkably, sparse deletion of *Arid1a* from *Arid1a*$^{fl/fl}$ EGFP+ cells did not disrupt their innervation of CC (solid arrow, *I*). Loss of ARID1A expression following sparse *Arid1a* deletion (open arrowheads, *G*) did not cell-autonomously cause axon misrouting defects.

axon guidance genes (Gene Ontology [GO]: 0007411) and 138 axon extension genes (GO: 0048675). This revealed an overlap of one axon guidance gene (*Ablim1*) and one axon extension gene (*Myo5b*), which were validated by ddRT-PCR (*SI Appendix*, Fig. S4*C*). Neither group was significantly overrepresented (P_{hyper} = 0.34 and 0.36, respectively).

To determine whether gene expression from particular cell types was preferentially affected in cKO-E, we performed intersectional analysis with single-cell RNA-seq (scRNA-seq) data from wild-type embryonic cortex (52). Unsupervised hierarchical clustering of cKO-E down-regulated genes based on scRNA-seq revealed a cluster with 46/91 genes (cluster 1) that are highly coexpressed at the level of single cells (Fig. 4*B*), suggesting that these down-regulated genes are normally expressed from one cell type. To validate this important finding, we performed intersectional analysis using an orthogonal dataset from wild-type E14.5 cortex (53), which revealed single-cell coexpression of 58/91 down-regulated genes (cluster A, *SI Appendix*, Fig. S4*D*). Remarkably, all 46 genes in cluster 1 were represented in cluster A. This complete overlap provided high confidence that the down-regulated genes in cKO-E reflected selective disruption of a single cell type.

To unbiasedly determine the identity of this cell type, we intersected the 46 cluster 1 genes with a rich spatiotemporal gene expression dataset covering over 1,200 brain subregions (54) using Enrichr (55). This revealed significant enrichment of genes selectively expressed in cortical layer 6b, an alternative nomenclature for SP (Fig. 4*C*). We next intersected cluster 1 genes with additional datasets orthogonal to the discovery data. We found overrepresentation of cluster 1 genes in genes preferentially expressed in the SP based on microdissection (31) (Fig. 4*D*). Intersection with a cell type–specific RNA-seq dataset (56) revealed overrepresentation of cluster 1 genes in "corticothalamic group 6" and "corticofugal group 11" (Fig. 4*D* and *SI Appendix*, Fig. S4*E*). Although SPNs were not specifically annotated in that dataset, marker membership suggests that these two groups comprise SPNs. Notably, cluster 1 genes showed no significant overlap with other major cell types (e.g., callosal neurons and corticospinal neurons), suggesting selective dysregulation of SPN genes in cKO-E. Available E14.5 in situ hybridization data (Genepaint) (57) and E15.5 EGFP transgene expression data (Gene Expression Nervous System Atlas [GENSAT]) (58) further supported that cluster 1 genes are expressed in the SP (Fig. 4*E*). Together, our analyses revealed selective disruption of SPN molecular identity following *Arid1a* deletion.

Consistent with disruption of SPN gene expression in cKO-E, anatomical development of SPNs was also altered. In P0 ctrl, RBFOX3-labeled SPNs were organized in a distinct, tight band positioned beneath CP (Fig. 4*F*). In cKO-E, the SP was disorganized and intermingled with CP. In ctrl, SPN marker CPLX3 (59) labeled a continuous band of SPNs (Fig. 4*G*). In cKO-E, gaps were present in the SP band (asterisks) and some CPLX3+ neurons were mispositioned in WM. In addition, CPLX3+ SPNs

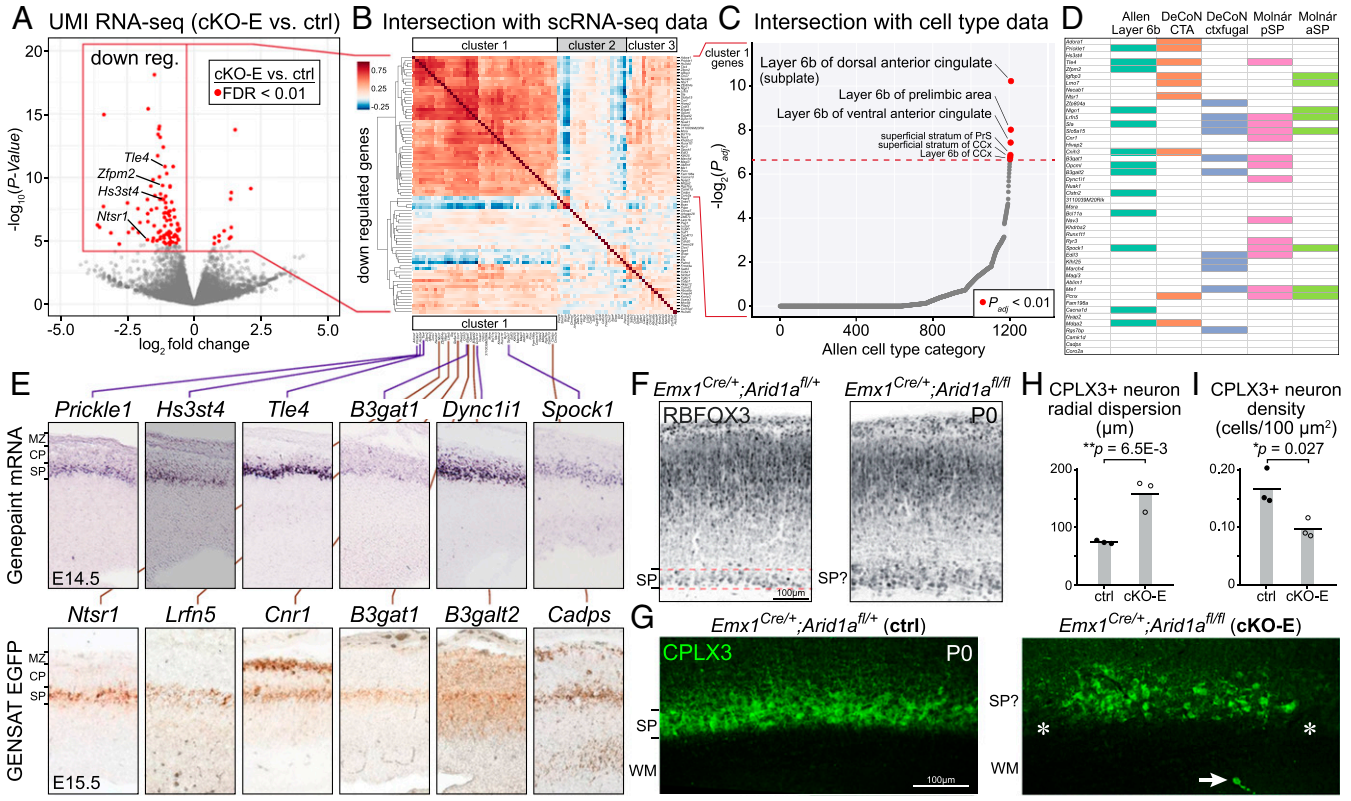

Fig. 4. Selective disruption of SPN gene expression following *Arid1a* deletion. (*A*) Volcano plot of UMI RNA-seq data comparing E15.5 cortex of cKO-E to ctrl littermates ($n = 6$ animals). For each gene, *P* value was calculated with likelihood ratio tests, and false discovery rate (FDR) was calculated using the Benjamini-Hochberg procedure. Of 103 differentially expressed genes (FDR < 0.01, red dots), 91 were down-regulated and 12 were up-regulated in cKO-E. (*B*) Intersectional analysis of significantly down-regulated genes with scRNA-seq data from wild-type embryonic forebrain (52). Unsupervised hierarchical clustering revealed a cluster of 46 down-regulated genes (cluster 1) highly coexpressed at the level of single cells, suggesting that they may be expressed from one cell type. (*C*) Intersectional analysis of the 46 genes in cluster 1 with a spatiotemporal gene expression dataset covering over 1,200 brain subregions (54). Cluster 1 showed significant overrepresentation of genes selectively expressed in layer 6b (alternative nomenclature for SP). (*D*) Intersectional analyses with orthogonal datasets (31, 54, 56). (*E*) SP expression of cluster 1 genes was confirmed by E14.5 in situ hybridization data from the Genepaint database and E15.5 EGFP transgene expression data from the GENSAT consortium (57, 58). (*F*) RBFOX3 immunostaining (black) on coronal sections of P0 ctrl revealed a distinct and organized SP band positioned beneath the cortical layers. In cKO-E, the SP band was unclearly defined and not distinct from CP. (*G*) CPLX3 immunostaining (green) on coronal P0 sections. In ctrl, CPLX3+ SPNs were organized into a discrete, continuous band. In cKO-E, CPLX3+ SPNs were more dispersed, characterized by gaps (asterisks), and sometimes aberrantly positioned in WM (arrow). (*H* and *I*) Quantification of CPLX3+ SPN radial dispersion and density at P0 (data are mean, two-tailed unpaired *t* test, $n = 3$ animals). pSP, posterior subplate; aSP, anterior subplate.

were significantly more dispersed (Fig. 4 *H* and *I*). Together, these data suggested that SPNs were present in cKO-E but anatomically disorganized and disrupted in cell type-dependent gene expression.

Altered Organization and Morphogenesis of Embryonic SPNs following *Arid1a* Deletion. The loss of SPN expression and noncell-autonomous axon phenotypes in cKO-E convergently suggested that *Arid1a* guidance functions may be centered on SP. SP ablation misroutes cortical axons and causes TCAs to prematurely invade CP in a manner reminiscent of cKO-E (Fig. 2) (17–19). Disrupted SP function also leads to defects in TCA crossing of the PSB and formation of cortical sensory maps (20, 21, 27, 28) similar to *Arid1a* deletion. We therefore characterized SPN characteristics that contribute to their circuit wiring functions.

SP mediates axon pathfinding during embryonic ages. We assessed embryonic SP organization by immunostaining of TUBB3 (TUJ1), a neuronal cytoskeleton marker that reveals embryonic cortical layers. At E14.5, TUBB3+ processes were horizontally organized in intermediate zone (IZ) in ctrl but invaded CP diagonally in cKO-E (Fig. 5*A*). In ctrl, analysis of MAP2, a somatodendritic marker, and NR4A2 (NURR1), an SPN and L6 neuron marker, revealed a distinct, continuous SP layer below CP (Fig. 5*B*). In cKO-E, SPNs showed abnormal clustering and cell-sparse gaps. Notably, MAP2-labeled dendrites aberrantly projected ventrally into IZ (red arrowheads, Fig. 5*B*). We further used the Tg(*Lpar1-EGFP*) transgene, which expresses EGFP in a subset of SPNs (58). In E16.5 and P0 cKO-E cortex, Lpar1-EGFP–labeled SPNs were characterized by cell-sparse gaps (asterisks) and some were aberrantly positioned in IZ or WM (arrows, Fig. 5*C* and *SI Appendix*, Fig. S5*A*).

To analyze SPN morphology, we leveraged an in vivo genome editing method that targets the actin gene *Actb* for sparse, whole-cell labeling. We used CRISPR-Cas9 to generate a DNA break at the C terminus of *Actb* and a homology-independent repair template containing a 3xHA epitope tag (50). Nonhomologous end joining that incorporates the template in forward orientation would lead to in-frame expression of ACTB-3xHA. To perform this assay in vivo, we used IUE to cotransfect CRISPR-Cas9, repair template, and CAG-mTagBFP2 into cortical NPCs at E11.5, the peak of SP neuronogenesis (schematized in Fig. 5*D*). Analyzed at E16.5, mTagBFP2 expression revealed successful targeting of SPNs (Fig. 5*E*). mTagBFP2-labeled SPNs were organized in a continuous narrow band positioned beneath CP in ctrl but showed aberrant clustering and gaps in cKO-E.

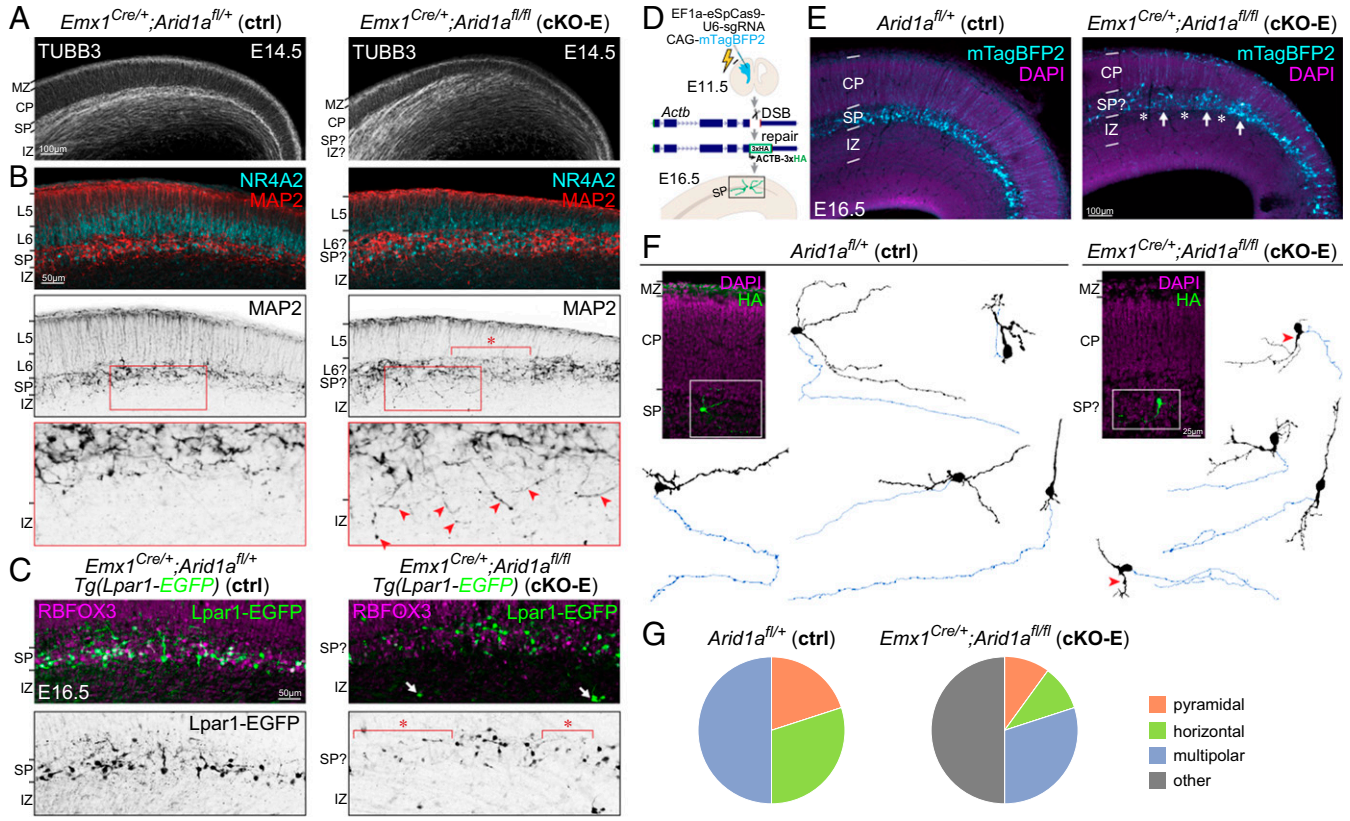

Fig. 5. Disrupted SP organization and SPN morphology following *Arid1a* deletion. (*A*) TUBB3 (TUJ1) immunostaining (white) on E14.5 sections. In ctrl, TUBB3+ processes were horizontally organized in IZ and SP and radially organized in CP. In cKO-E, TUBB3+ axons became defasciculated in IZ and invaded CP diagonally. (*B*) MAP2 (red, black) and NR4A2 (cyan) immunostaining on E14.5 sections. In ctrl, MAP2+/NR4A2+ SPNs were organized within a clearly delineated layer below CP. In cKO-E, SPNs were characterized by abnormal clustering and cell-sparse gaps (asterisk), and misoriented MAP2+ dendrites aberrantly projected ventrally into IZ (red arrowheads, *Inset*). (*C*) RBFOX3 (NEUN) immunostaining (magenta) on E16.5 brains carrying the *Lpar1-EGFP* transgene. In cKO-E, Lpar1-EGFP+ SPNs (green, black) were characterized by cell-sparse gaps (asterisks), and some Lpar1-EGFP+ neurons were aberrantly positioned in IZ (arrows). (*D*) Schematic illustration of sparse SPN labeling by in utero genome editing. A DNA break was induced by CRISPR-Cas9 within the coding region of *Actb* near the C terminus. A reporter repair template was designed such that correct repair would lead to ACTB-3xHA expression. CRISPR-Cas9, reporter repair, and mTagBFP2 expression constructs were cotransfected into cortical NPCs at E11.5 by IUE. Electroporated brains were analyzed at E16.5. (*E*) mTagBFP2 (cyan) successfully targeted SPNs in electroporated brains. In cKO-E, labeled SPNs showed disorganization with abnormal cell clusters (arrows) and cell-sparse gaps (asterisks). (*F*) HA immunostaining (green) revealed complete morphology of ACTB-3xHA-labeled SPNs. Neurons were reconstructed based on confocal Z-stacks. Dendrites are indicated in black. Axons are indicated in blue. In cKO-E, some SPNs were characterized by a dendrite ventrally directed into IZ (red arrowheads). (*G*) Quantification of SPN morphological subclasses.

Reconstruction of confocal Z-stacks revealed diverse morphologies in ACTB-3xHA-labeled SPNs in ctrl, including pyramidal, horizontal, and multipolar (Fig. 5 *F* and *G*). Diverse subclasses in SPN morphology have been documented (7, 60, 61), although embryonic SPN morphologies have not been extensively characterized. In cKO-E, SPN morphologies were also diverse; however, many deviated from the morphological subclasses observed in normal SP. Some SPNs were characterized by a ventrally directed dendrite extending into IZ (red arrowheads, Fig. 5*F*). Unlike SPNs, cKO-E pyramidal neurons were morphologically indistinguishable from ctrl (*SI Appendix*, Fig. S5*B*). Thus, our data revealed a cell type-dependent *Arid1a* function in SPN morphogenesis.

Disrupted Extracellular Matrix and SP Axon-TCA Cofasciculation following *Arid1a* Deletion. SPNs are the first neurons to extend corticofugal axons. These descending axons contribute to guidance of thalamocortical ascending axons via cofasciculation in a model known as the "handshake hypothesis" (25, 62) (schematized in Fig. 6*A*). To visualize SPN corticofugal axons, we used the Tg(*Golli-tau-EGFP*) transgene, which expresses TAU (τ)EGFP in SPNs and L6 neurons (63). In E15.5 ctrl, an abundance of τEGFP+ axons had extended across the PSB. In subpallium, these descending axons were closely apposed with NTNG1+ TCAs, consistent with cofasciculation (solid arrowheads, Fig. 6*B*). In contrast, in cKO-E, subpallial innervation by τEGFP+ axons was attenuated and no cofasciculation with NTNG1+ axons was found (open arrowheads, Fig. 6*B*). By E17.5, extensive cofasciculation of τEGFP+ and NTNG1+ axons was present in ctrl but was largely absent from cKO-E (Fig. 6*C*). In P0 cKO-E, some NTNG1+ axons followed the aberrant trajectories of misrouted τEGFP+ axons, whereas other NTNG1+ axons, without cofasciculation, were misrouted (*SI Appendix*, Fig. S6*A*). Concomitant with loss of cofasciculation in cKO-E, NTNG1+ TCAs were consistently unable to correctly traverse the PSB (arrows, Fig. 6 *B* and *C* and *SI Appendix*, Fig. S6*B*, 5/5 animals), entered cortex via a narrow medial path, became defasciculated in IZ, and prematurely invaded CP. Notably, earlier in development in cKO-E, TCAs did not show misrouting defects at E13.5, prior to PSB crossing (*SI Appendix*, Fig. S6*C*), suggesting that their misrouting followed the loss of subpallial cofasciculation with SP axons. Our data are thus consistent with the model posited by the "handshake hypothesis" (7).

SPNs are rich in extracellular matrix (64, 65), and secreted molecules derived from SPNs are thought to guide axons traversing the SP (66). During normal pathfinding, TCAs innervate

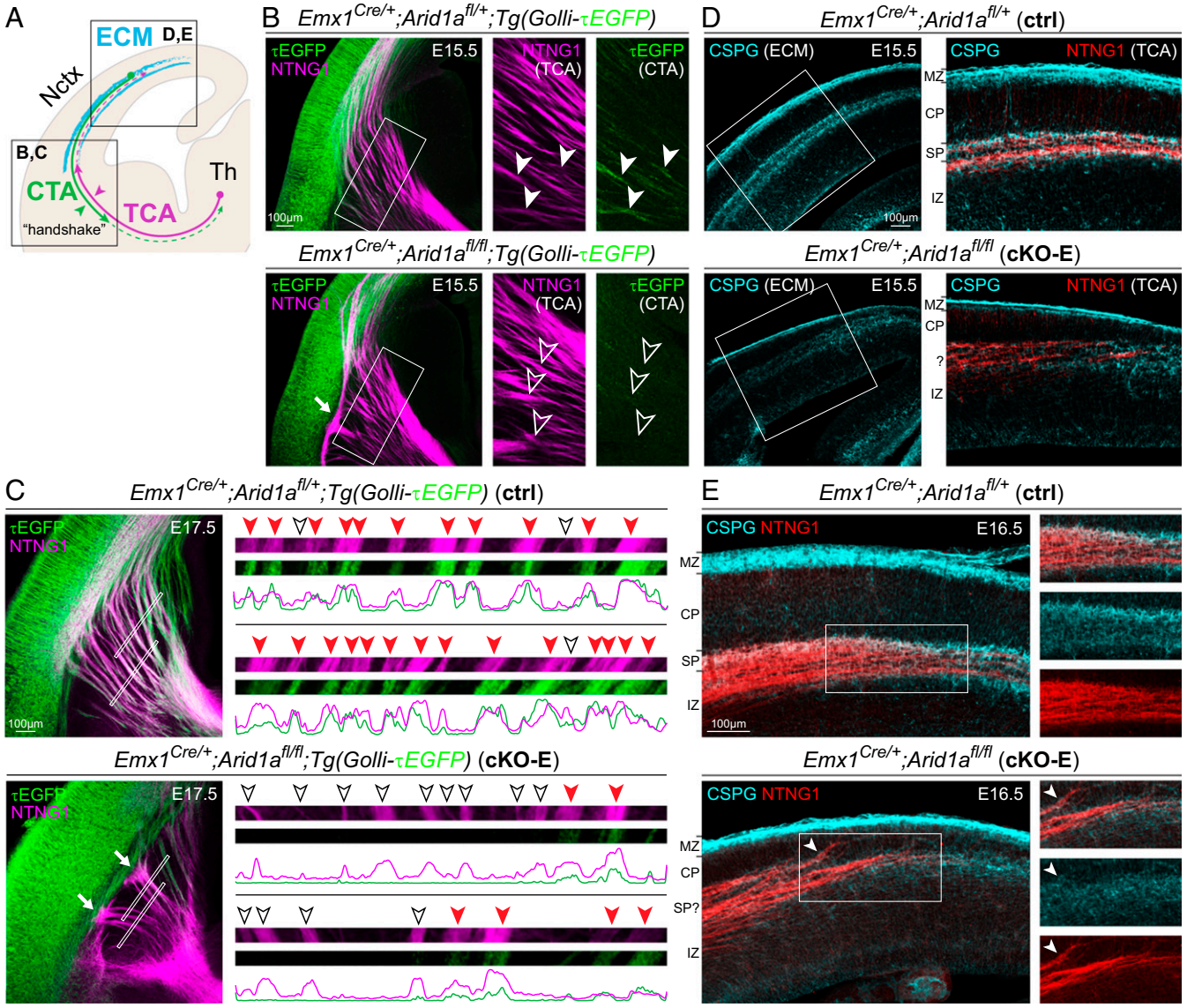

Fig. 6. Aberrant SPN axon projections and extracellular matrix following *Arid1a* deletion. (*A*) Schematic illustration of SPN functions. (*B* and *C*) NTNG1 immunostaining (magenta) on E15.5 (*B*) and E17.5 (*C*) brains carrying the *Golli-τEGFP* transgene. In E15.5 ctrl, τEGFP+ (green) descending axons from SPNs closely cofasciculated (solid arrowheads) with ascending NTNG1+ TCAs (magenta). In E15.5 cKO-E, τEGFP+ axons largely have not descended across the PSB. Ascending NTNG1+ TCAs, without cofasciculation with descending τEGFP+ axons (open arrowheads), did not cross the PSB along the normal trajectory and formed an aberrant bundle parallel to the boundary (solid arrow). In E17.5 ctrl, we found frequent cofasciculation (red arrowheads, *Inset*) of τEGFP+ and NTNG1+ axons, consistent with the "handshake hypothesis." In E17.5 cKO-E, most NTNG1+ TCAs did not cofasciculate with τEGFP+ axons (open arrowheads) and were unable to cross the PSB (solid arrows). (*D* and *E*) CSPG (cyan) and NTNG1 (red) immunostaining on E15.5 (*D*) and E16.5 (*E*) brain sections. In ctrl, NTNG1+ TCAs tangentially traversed the embryonic cortex within a SP/IZ corridor neatly delineated by extracellular matrix (ECM) component CSPG. In cKO-E, CSPG expression was reduced and the CSPG corridor had collapsed. NTNG1+ TCAs were not confined within SP/IZ, deviated from their normal trajectory, and prematurely invaded CP (arrowhead). CTA, corticothalamic axon.

cortex via a WM corridor delineated by extracellular matrix component chondroitin sulfate proteoglycan (CSPG) (29), which we observed in E15.5 and E16.5 ctrl (Fig. 6 *D* and *E*). In cKO-E, CSPG expression was reduced, and the CSPG corridor had collapsed (Fig. 6 *D* and *E*). Concomitant with CSPG corridor disruption, NTNG1+ TCAs were not confined within WM, deviated from their normal trajectory, and prematurely invaded CP. Together, our analyses revealed deficits in SPN morphogenesis, SP axon cofasciculation with TCAs, and SP extracellular matrix following *Arid1a* deletion.

SP-Spared CP Deletion of *Arid1a* Extensively Abrogated Axon Misrouting. To empirically test the hypothesis that SPNs mediate the axon guidance functions of *Arid1a*, we sought to determine whether *Arid1a* expression in SPNs was sufficient to support axon pathfinding from cortical neurons that lacked *Arid1a*. We generated an *Arid1a* cKO using Tg(*hGFAP-Cre*) (67). Tg(*hGFAP-Cre*) mediates Cre recombination in cortical NPCs starting at E12.5, after the majority of SPNs have been generated (Fig. 7*A* and *SI Appendix*, Fig. S7*A*); therefore, *Arid1a* would be deleted from CP neurons, whereas SPNs would be spared. SP-spared cortical deletion was confirmed by ARID1A immunostaining in Tg(*hGFAP-Cre*);*Arid1a*$^{fl/fl}$ (cKO-hG) (Fig. 7*A*). Importantly, Tg(*hGFAP-Cre*) mediated *Arid1a* deletion from L6 neurons by E13.5 (Fig. 7*A* and *SI Appendix*, Fig. S7 *B* and *C*), thus uncoupling the effects of SPNs from molecularly similar L6 neurons. In P0 cKO-hG, sparing SPNs from *Arid1a* deletion led to correct anatomical formation of the SP band (Fig. 7 *B* and *C*). Next,

we analyzed cortical axon tracts using Cre-dependent reporter $ROSA^{tdTomato}$ (Fig. 7*B*). Remarkably, in cKO-hG, axons arising from tdTomato-labeled, *Arid1a*-deleted, CP neurons correctly formed CC and projected into contralateral cortex (Fig. 7 *B* and *C*). In addition to intracortical axons, TCAs were also normal in pathfinding in cKO-hG. At P7, CO staining on flattened cKO-hG cortices revealed typical organization of barrel cortex (Fig. 7*D* and *SI Appendix*, Fig. S7*D*, 3/3 animals), which was confirmed by NTNG1 (Fig. 7*D*). Thus, *Arid1a* expression in SPNs was sufficient for normal SP organization, callosum formation, and TCA targeting.

Next, we assessed whether correct formation of axon tracts in cKO-hG was coincident with normal SP wiring functions. At E15.5, MAP2 immunostaining in cKO-hG revealed typical organization of SPNs indistinguishable from ctrl (Fig. 7*E*). NTNG1+ TCAs entered the cortex along a normal trajectory without premature invasion of CP (Fig. 7*E*). *Golli-τEGFP*-labeled corticofugal axons descended without defect (*SI Appendix*, Fig. S7*E*) and extensively cofasciculated with NTNG1-labeled TCAs in E15.5 cKO-hG (Fig. 7*F*). Furthermore, a CSPG corridor delineating the path of TCAs was present (Fig. 7*G*). Therefore, despite absence of ARID1A from CP neurons, SP ARID1A expression was sufficient for normal SP organization, SP axon-TCA cofasciculation, and extracellular matrix. Consistent with these wiring functions, SP *Arid1a* sufficiently enabled normal callosum formation, TCA targeting, and whisker barrel development.

Together, *Arid1a* cKO-E and cKO-hG supported examination of cell- and noncell-autonomous *Arid1a* functions. In SPNs, *Arid1a* was required for transcription of SP genes and gave rise to SPN organization, cofasciculation with TCAs, and extracellular matrix. By regulating the identity and functions of SPNs, *Arid1a* noncell-autonomously controlled the wiring of callosal and thalamocortical connectivities via the axon guidance roles of SP (schematized in *SI Appendix*, Fig. S8). *Arid1a* is thus a central regulator of multiple SP-dependent axon guidance mechanisms essential to cortical circuit assembly.

Discussion

Despite the central role of SPNs in cortical circuit assembly and their potential contribution to neurodevelopmental disorders (5, 22, 24), they are relatively understudied compared to their CP counterparts. Previous studies have focused on SP-enriched genes (23, 31) and characterized important molecular determinants of SPN specification, migration, and axon projections (32–38). The severe axon misrouting phenotypes of SP ablation (17–19) are, however, not broadly recapitulated in these genetic mutants. Here, we leverage cortical *Arid1a* deletion, which causes axon misrouting defects strikingly reminiscent of SP ablation, to gain mechanistic insights into the noncell-autonomous wiring functions of SPNs in assembling cortical connectivities.

Cortical *Arid1a* deletion and previous experimental SP ablation (17–20) phenotypically converge on misrouted TCAs, which prematurely invade CP and ultimately fail to innervate their L4 targets with correct topology. Several aspects of SP function may contribute to correct TCA pathfinding. First, the "handshake hypothesis" posits that close cofasciculation between descending SP axons and ascending TCAs is important for guidance of both tracts and formation of reciprocal connectivity (25, 62, 68). Following *Arid1a* deletion in cKO-E, SP corticofugal axons are markedly reduced, and their cofasciculation with TCAs is lost. Consistent with the "handshake hypothesis," TCAs, in the absence of cofasciculation, are impaired in PSB crossing, enter cortex via a narrow medial path, and become defasciculated and misrouted after entering the cortex. These phenotypes are reminiscent of misrouting defects that follow disrupted SP function (27, 28) or abnormal shifting of SP due to piriform cortex expansion (69). Second, SP is characterized by a rich extracellular matrix (4, 44), which contributes to axon guidance by interacting with growth cones and supporting signaling (5). During circuit formation, cortical afferent and efferent axons extend along a WM corridor delineated by matrix component CSPG (29). Following cortical *Arid1a* deletion, CSPG expression is reduced and the corridor collapses. Concomitantly, TCAs become defasciculated and prematurely invade CP, a phenotype reminiscent of SP ablation (17). Notably, sparing SPNs from *Arid1a* deletion in cKO-hG is sufficient to support both SP axon-TCA cofasciculation and the CSPG corridor and enables correct TCA pathfinding. The roles of *Arid1a* in thalamocortical tract formation are therefore centered on SPNs. Interestingly, corticothalamic axons from CP neurons are largely intact following *Arid1a* deletion in cKO-E, despite reduced SP-thalamic axons. Thus, we do not find an *Arid1a*-dependent pioneering role for SP axons in guiding corticothalamic axons from CP neurons.

Unlike the better-known roles of SPNs in TCA guidance, SP contribution to intracortical tract development is less established. Early studies suggest that SPNs pioneer CC formation by extending the first callosal axons (60, 70–72). Some subsequent studies, however, find this possibility unlikely (73, 74). We find that pancortical *Arid1a* deletion in cKO-E leads to CC agenesis and mistargeting of intracortical axons. Sparse *Arid1a* deletion, however, does not autonomously misroute callosal axons, indicating that callosal agenesis is a noncell-autonomous consequence of pancortical *Arid1a* deletion. Remarkably, SP expression of *Arid1a* in cKO-hG is sufficient for callosum formation. Thus, we unequivocally establish that SP function is essential to callosum development. We note that Tg(*hGFAP-Cre*) is active in indusium griseum and glial wedge (75, 76). It is therefore unlikely that *Arid1a* expression in these structures could contribute to callosum formation in cKO-hG. Diverse developmental disorders are characterized by agenesis or dysgenesis of CC (77). Our study highlights a potential contribution of SP dysfunction to callosal defects in disease.

One barrier to molecular study of SP function is the lack of specific genetic access to embryonic SPNs during critical stages of circuit wiring. Although several published Cre lines show SPN specificity, Cre expression occurs too late for study of circuit development (78). Here, we describe a genetic strategy to target SPNs. We find that $Emx1^{Cre}$ mediates gene deletion from all cortical NPCs, including those that give rise to SPNs, whereas Tg(*hGFAP-Cre*) mediates deletion from NPCs after SPNs have been generated. Importantly, Tg(*hGFAP-Cre*) mediates recombination in a majority of L6 neurons, thereby enabling potential effects of SPNs to be uncoupled from closely related L6 neurons. By comparing "pancortical deletion" ($Emx1^{Cre}$) versus "subplate-spared deletion" (Tg[*hGFAP-Cre*]), this approach enables interrogation of gene necessity and sufficiency in SP-mediated circuit wiring.

In cortical NPCs, we find that *Arid1a* deletion selectively disrupts SPN gene expression. Despite ubiquitous ARID1A expression during cortical development, the effects of *Arid1a* deletion are surprisingly cell type-dependent. A recent study showed that *Arid1b* expression following *Arid1a* depletion partially supported BAF function (45). In our cKO-E, expression of *Arid1b* may have attenuated the effects of *Arid1a* loss from CP neurons, thus contributing to SP-selective deficits.

Recent human genetic findings have convergently implicated altered chromatin function in disorders of brain development (79, 80). These studies identified loss-of-function mutations in *ARID1A* in intellectual disability, autism spectrum disorder, and Coffin-Siris syndrome, a developmental disorder characterized by callosal dysgenesis (39). The mechanisms by which chromatin dysregulation contributes to brain disorders are an active field of study. An important implication of our work is that deficits in SPNs may be an underappreciated contributor to neural circuit miswiring in neurodevelopmental disorders, including those associated with chromatin dysregulation.

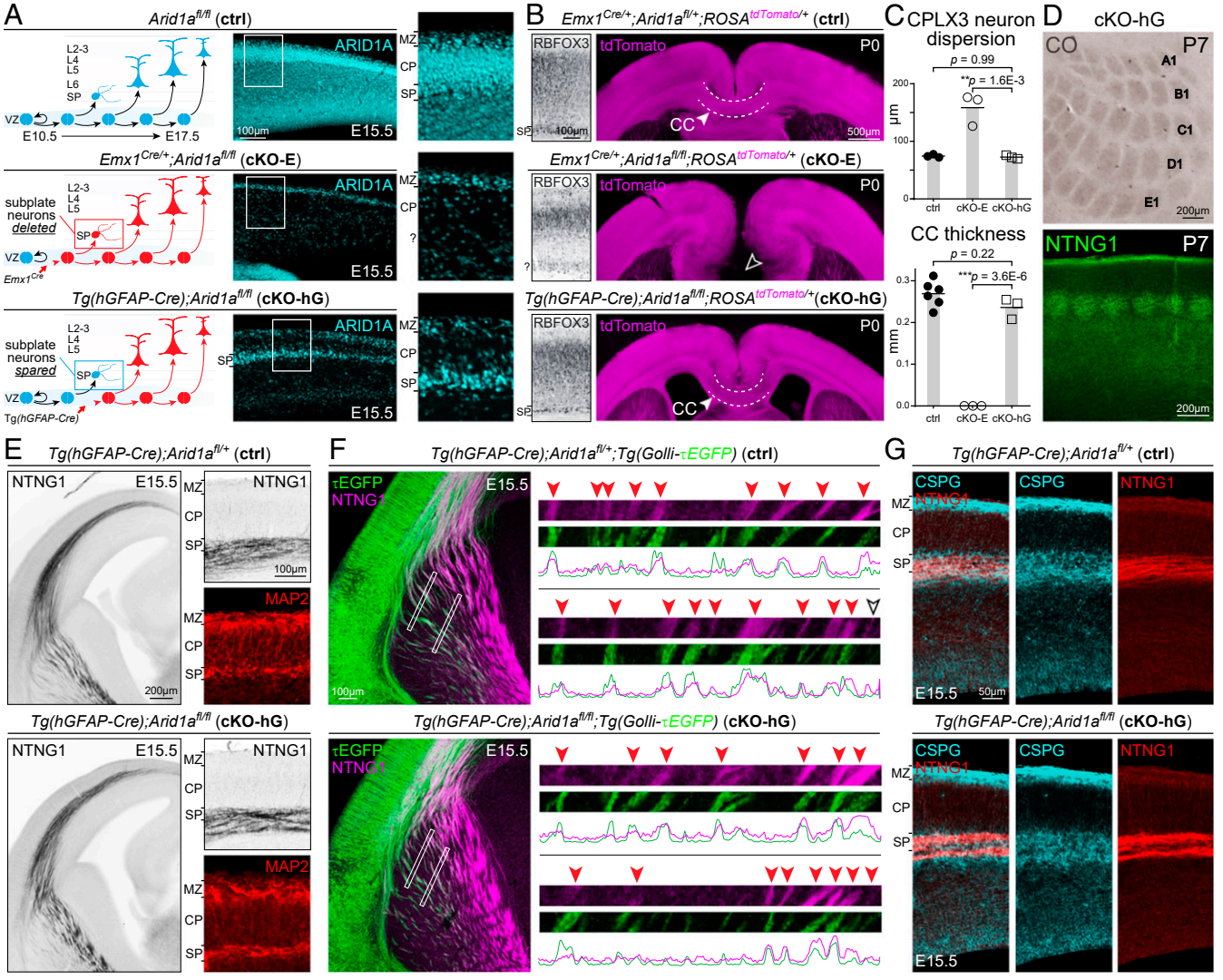

Fig. 7. SP-spared CP deletion of *Arid1a*. (*A*) Schematic illustration of SP-spared CP deletion of *Arid1a*. *Emx1*^{Cre} mediates Cre recombination in cortical NPCs starting at E10.5, prior to SPN genesis. ARID1A immunostaining (cyan) in E15.5 cKO-E revealed loss of ARID1A from SPNs and CP neurons. Tg(*hGFAP-Cre*) mediates Cre recombination in cortical NPCs starting at E12.5, after the majority of SPNs have been generated. In E15.5 Tg(*hGFAP-Cre*);*Arid1a*$^{fl/fl}$ (cKO-hG), ARID1A was lost from CP neurons but present in SPNs. (*B*) SP and axon tract analyses on P0 brain sections. RBFOX3 immunostaining revealed in cKO-hG an organized, distinct SP band positioned just beneath CP. tdTomato (magenta) was expressed Cre dependently from *ROSA*^{tdTomato}, enabling visualization of cortical axons. Callosal agenesis (open arrowhead) was observed in cKO-E. However, the CC formed without gross defect in cKO-hG (solid arrowhead, 3/3 animals). (*C*) Quantitative analyses revealed no significant changes in CPLX3+ SPN radial dispersion or callosal thickness at midline in cKO-hG compared to ctrl (data are mean, ANOVA with Tukey's post hoc test, $n \geq 3$ animals). (*D*) Whisker barrels in P7 primary somatosensory cortex were visualized by CO staining (brown) on flattened cortices and NTNG1 immunostaining (green) on coronal sections. Whisker barrels formed without defect in cKO-hG (3/3 animals). (*E*) Analysis of TCAs and SPNs in E15.5 cortex. In cKO-hG, NTNG1+ TCAs extended along a normal trajectory across the PSB, without forming an aberrant bundle parallel to the boundary. Upon reaching the cortex, NTNG1+ axons correctly paused within SP without prematurely invading CP in cKO-hG. MAP2 immunostaining (red) revealed that SPNs were organized within a continuous and clearly delineated layer below CP. (*F*) NTNG1 immunostaining (magenta) on E15.5 brains carrying the *Golli-τEGFP* transgene. In cKO-hG, τEGFP+ (green) descending axons from SPNs closely cofasciculated (red arrowheads) with ascending NTNG1+ TCAs (magenta). (*G*) CSPG (cyan) and NTNG1 (red) immunostaining on E15.5 brain sections. In cKO-hG, NTNG1+ TCAs traveled within an SP/IZ corridor neatly delineated by extracellular matrix component CSPG in a manner indistinguishable from ctrl.

Materials and Methods

Further experimental details can be found in *SI Appendix*, *Supplementary Materials and Methods*.

Animals. All experiments were carried out in compliance with a protocol approved by the University of Michigan Institutional Animal Care & Use Committee. Strain details are provided in *SI Appendix*.

IUE. Approximately 2 μL DNA was transfected into VZ NPCs by IUE. Experimental details are provided in *SI Appendix*.

UMI RNA-Seq. Data were deposited to National Center for Biotechnology Information Gene Expression Omnibus (NCBI GEO): GSE163273. Details are provided in *SI Appendix*.

Data Availability. RNA-seq data have been deposited in NCBI GEO (GSE163273).

ACKNOWLEDGMENTS. We thank members of the Kwan laboratory for discussions and comments on the study, critical reading of the manuscript, and scientific discussions and colleagues in the Michigan Neuroscience Institute (MNI) and Department of Human Genetics for insightful suggestions. This

work was supported by the NIH (R01 NS097525 to K.Y.K., F31 NS110206 to D.Z.D., and T32 GM007544 to O.H.F.), the Brain Research Foundation (BRFSG-2016-04 to K.Y.K.), March of Dimes Foundation (No. 5-FY15-33 to K.Y.K.), and Simons Foundation Autism Research Initiative (402213 and 324586 to K.Y.K.).

1. K. L. Allendoerfer, C. J. Shatz, The subplate, a transient neocortical structure: Its role in the development of connections between thalamus and cortex. *Annu. Rev. Neurosci.* **17**, 185–218 (1994).
2. S. K. McConnell, A. Ghosh, C. J. Shatz, Subplate neurons pioneer the first axon pathway from the cerebral cortex. *Science* **245**, 978–982 (1989).
3. S. K. McConnell, A. Ghosh, C. J. Shatz, Subplate pioneers and the formation of descending connections from cerebral cortex. *J. Neurosci.* **14**, 1892–1907 (1994).
4. I. Kostović, P. Rakic, Developmental history of the transient subplate zone in the visual and somatosensory cortex of the macaque monkey and human brain. *J. Comp. Neurol.* **297**, 441–470 (1990).
5. A. Hoerder-Suabedissen, Z. Molnár, Development, evolution and pathology of neocortical subplate neurons. *Nat. Rev. Neurosci.* **16**, 133–146 (2015).
6. W. Z. Wang *et al*., Subplate in the developing cortex of mouse and human. *J. Anat.* **217**, 368–380 (2010).
7. Z. Molnár, R. Adams, A. M. Goffinet, C. Blakemore, The role of the first postmitotic cortical cells in the development of thalamocortical innervation in the reeler mouse. *J. Neurosci.* **18**, 5746–5765 (1998).
8. Z. Molnár, H. J. Luhmann, P. O. Kanold, Transient cortical circuits match spontaneous and sensory-driven activity during development. *Science* **370**, eabb2153 (2020).
9. I. Kostović, M. E. Molliver, A new interpretation of the laminar development of cerebral cortex: Synaptogenesis in different layers of neopallium in the human fetus. *Anat. Rec.* **178**, 395 (1974).
10. I. Kostović, The enigmatic fetal subplate compartment forms an early tangential cortical nexus and provides the framework for construction of cortical connectivity. *Prog. Neurobiol.* **194**, 101883 (2020).
11. Z. Molnár *et al*., New insights into the development of the human cerebral cortex. *J. Anat.* **235**, 432–451 (2019).
12. K. Y. Kwan, N. Sestan, E. S. Anton, Transcriptional co-regulation of neuronal migration and laminar identity in the neocortex. *Development* **139**, 1535–1546 (2012).
13. P. O. Kanold, H. J. Luhmann, The subplate and early cortical circuits. *Annu. Rev. Neurosci.* **33**, 23–48 (2010).
14. E. Friauf, S. K. McConnell, C. J. Shatz, Functional synaptic circuits in the subplate during fetal and early postnatal development of cat visual cortex. *J. Neurosci.* **10**, 2601–2613 (1990).
15. J. M. Wess, A. Isaiah, P. V. Watkins, P. O. Kanold, Subplate neurons are the first cortical neurons to respond to sensory stimuli. *Proc. Natl. Acad. Sci. U.S.A.* **114**, 12602–12607 (2017).
16. C. Ohtaka-Maruyama *et al*., Synaptic transmission from subplate neurons controls radial migration of neocortical neurons. *Science* **360**, 313–317 (2018).
17. A. Ghosh, C. J. Shatz, A role for subplate neurons in the patterning of connections from thalamus to neocortex. *Development* **117**, 1031–1047 (1993).
18. A. Ghosh, A. Antonini, S. K. McConnell, C. J. Shatz, Requirement for subplate neurons in the formation of thalamocortical connections. *Nature* **347**, 179–181 (1990).
19. A. Ghosh, C. J. Shatz, Involvement of subplate neurons in the formation of ocular dominance columns. *Science* **255**, 1441–1443 (1992).
20. P. O. Kanold, C. J. Shatz, Subplate neurons regulate maturation of cortical inhibition and outcome of ocular dominance plasticity. *Neuron* **51**, 627–638 (2006).
21. P. O. Kanold, P. Kara, R. C. Reid, C. J. Shatz, Role of subplate neurons in functional maturation of visual cortical columns. *Science* **301**, 521–525 (2003).
22. M. Serati *et al*., The role of the subplate in schizophrenia and autism: A systematic review. *Neuroscience* **408**, 58–67 (2019).
23. A. Hoerder-Suabedissen *et al*., Expression profiling of mouse subplate reveals a dynamic gene network and disease association with autism and schizophrenia. *Proc. Natl. Acad. Sci. U.S.A.* **110**, 3555–3560 (2013).
24. I. Kostović, M. Judaš, G. Sedmak, Developmental history of the subplate zone, subplate neurons and interstitial white matter neurons: Relevance for schizophrenia. *Int. J. Dev. Neurosci.* **29**, 193–205 (2011).
25. C. Blakemore, Z. Molnár, Factors involved in the establishment of specific interconnections between thalamus and cerebral cortex. *Cold Spring Harb. Symp. Quant. Biol.* **55**, 491–504 (1990).
26. Z. Molnár, C. Blakemore, How do thalamic axons find their way to the cortex? *Trends Neurosci.* **18**, 389–397 (1995).
27. D. Magnani, K. Hasenpusch-Theil, T. Theil, Gli3 controls subplate formation and growth of cortical axons. *Cereb. Cortex* **23**, 2542–2551 (2013).
28. Y. Chen, D. Magnani, T. Theil, T. Pratt, D. J. Price, Evidence that descending cortical axons are essential for thalamocortical axons to cross the pallial-subpallial boundary in the embryonic forebrain. *PLoS One* **7**, e33105 (2012).
29. A. R. Bicknese, A. M. Sheppard, D. D. O'Leary, A. L. Pearlman, Thalamocortical axons extend along a chondroitin sulfate proteoglycan-enriched pathway coincident with the neocortical subplate and distinct from the efferent path. *J. Neurosci.* **14**, 3500–3510 (1994).
30. D. J. Price, S. Aslam, L. Tasker, K. Gillies, Fates of the earliest generated cells in the developing murine neocortex. *J. Comp. Neurol.* **377**, 414–422 (1997).
31. F. M. Oeschger *et al*., Gene expression analysis of the embryonic subplate. *Cereb. Cortex* **22**, 1343–1359 (2012).
32. W. Han *et al*., TBR1 directly represses Fezf2 to control the laminar origin and development of the corticospinal tract. *Proc. Natl. Acad. Sci. U.S.A.* **108**, 3041–3046 (2011).
33. R. F. Hevner *et al*., Tbr1 regulates differentiation of the preplate and layer 6. *Neuron* **29**, 353–366 (2001).
34. S. Y. X. Tiong *et al*., *Kcnab1* is expressed in subplate neurons with unilateral long-range inter-areal projections. *Front. Neuroanat.* **13**, 39 (2019).
35. Y. Arai *et al*., Evolutionary gain of Dbx1 expression drives subplate identity in the cerebral cortex. *Cell Rep.* **29**, 645–658.e5 (2019).
36. L. Ratie *et al*., Loss of Dmrt5 affects the formation of the subplate and early corticogenesis. *Cereb. Cortex* **30**, 3296–3312 (2019).
37. K. Y. Kwan *et al*., SOX5 postmitotically regulates migration, postmigratory differentiation, and projections of subplate and deep-layer neocortical neurons. *Proc. Natl. Acad. Sci. U.S.A.* **105**, 16021–16026 (2008).
38. W. L. McKenna *et al*., Tbr1 and Fezf2 regulate alternate corticofugal neuronal identities during neocortical development. *J. Neurosci.* **31**, 549–564 (2011).
39. T. Kosho, N. Okamoto; Coffin-Siris Syndrome International Collaborators, Genotype-phenotype correlation of Coffin-Siris syndrome caused by mutations in SMARCB1, SMARCA4, SMARCE1, and ARID1A. *Am. J. Med. Genet. C. Semin. Med. Genet.* **166C**, 262–275 (2014).
40. I. Olave, W. Wang, Y. Xue, A. Kuo, G. R. Crabtree, Identification of a polymorphic, neuron-specific chromatin remodeling complex. *Genes Dev.* **16**, 2509–2517 (2002).
41. E. Y. Son, G. R. Crabtree, The role of BAF (mSWI/SNF) complexes in mammalian neural development. *Am. J. Med. Genet. C. Semin. Med. Genet.* **166C**, 333–349 (2014).
42. X. Gao *et al*., ES cell pluripotency and germ-layer formation require the SWI/SNF chromatin remodeling component BAF250a. *Proc. Natl. Acad. Sci. U.S.A.* **105**, 6656–6661 (2008).
43. J. A. Gorski *et al*., Cortical excitatory neurons and glia, but not GABAergic neurons, are produced in the Emx1-expressing lineage. *J. Neurosci.* **22**, 6309–6314 (2002).
44. I. Kostović, M. Judas, The development of the subplate and thalamocortical connections in the human foetal brain. *Acta Paediatr.* **99**, 1119–1127 (2010).
45. M. Trizzino *et al*., The tumor suppressor ARID1A controls global transcription via pausing of RNA polymerase II. *Cell Rep.* **23**, 3933–3945 (2018).
46. R. Mathur *et al*., ARID1A loss impairs enhancer-mediated gene regulation and drives colon cancer in mice. *Nat. Genet.* **49**, 296–302 (2017).
47. N. Antón-Bolaños, A. Espinosa, G. López-Bendito, Developmental interactions between thalamus and cortex: A true love reciprocal story. *Curr. Opin. Neurobiol.* **52**, 33–41 (2018).
48. A. Routh, S. R. Head, P. Ordoukhanian, J. E. Johnson, ClickSeq: Fragmentation-free next-generation sequencing via click ligation of adaptors to stochastically terminated 3′-azido cDNAs. *J. Mol. Biol.* **427**, 2610–2616 (2015).
49. L. Shi, A. Qalieh, M. M. Lam, J. M. Keil, K. Y. Kwan, Robust elimination of genome-damaged cells safeguards against brain somatic aneuploidy following Knl1 deletion. *Nat. Commun.* **10**, 2588 (2019).
50. J. M. Keil *et al*., Symmetric neural progenitor divisions require chromatin-mediated homologous recombination DNA repair by Ino80. *Nat. Commun.* **11**, 3839 (2020).
51. M. D. Robinson, D. J. McCarthy, G. K. Smyth, edgeR: A Bioconductor package for differential expression analysis of digital gene expression data. *Bioinformatics* **26**, 139–140 (2010).
52. S. A. Yuzwa *et al*., Developmental emergence of adult neural stem cells as revealed by single-cell transcriptional profiling. *Cell Rep.* **21**, 3970–3986 (2017).
53. L. Loo *et al*., Single-cell transcriptomic analysis of mouse neocortical development. *Nat. Commun.* **10**, 134 (2019).
54. S. M. Sunkin *et al*., Allen brain atlas: An integrated spatio-temporal portal for exploring the central nervous system. *Nucleic Acids Res.* **41**, D996–D1008 (2013).
55. M. V. Kuleshov *et al*., Enrichr: A comprehensive gene set enrichment analysis web server 2016 update. *Nucleic Acids Res.* **44**, W90–W97 (2016).
56. B. J. Molyneaux *et al*., DeCoN: Genome-wide analysis of in vivo transcriptional dynamics during pyramidal neuron fate selection in neocortex. *Neuron* **85**, 275–288 (2015).
57. A. Visel, C. Thaller, G. Eichele, GenePaint.org: An atlas of gene expression patterns in the mouse embryo. *Nucleic Acids Res.* **32**, D552–D556 (2004).
58. S. Gong *et al*., A gene expression atlas of the central nervous system based on bacterial artificial chromosomes. *Nature* **425**, 917–925 (2003).
59. A. Hoerder-Suabedissen *et al*., Novel markers reveal subpopulations of subplate neurons in the murine cerebral cortex. *Cereb. Cortex* **19**, 1738–1750 (2009).
60. A. Hoerder-Suabedissen, Z. Molnár, Morphology of mouse subplate cells with identified projection targets changes with age. *J. Comp. Neurol.* **520**, 174–185 (2012).
61. J. A. De Carlos, D. D. O'Leary, Growth and targeting of subplate axons and establishment of major cortical pathways. *J. Neurosci.* **12**, 1194–1211 (1992).
62. Z. Molnár, S. Garel, G. López-Bendito, P. Maness, D. J. Price, Mechanisms controlling the guidance of thalamocortical axons through the embryonic forebrain. *Eur. J. Neurosci.* **35**, 1573–1585 (2012).
63. M. C. Piñon, A. Jethwa, E. Jacobs, A. Campagnoni, Z. Molnár, Dynamic integration of subplate neurons into the cortical barrel field circuitry during postnatal development in the Golli-tau-eGFP (GTE) mouse. *J. Physiol.* **587**, 1903–1915 (2009).
64. I. Kostović, I. Ž. Išasegi, Ž. Krsnik, Sublaminar organization of the human subplate: Developmental changes in the distribution of neurons, glia, growing axons and extracellular matrix. *J. Anat.* **235**, 481–506 (2019).
65. M. Judas, N. J. Milosević, M. R. Rasin, M. Heffer-Lauc, I. Kostović, Complex patterns and simple architects: Molecular guidance cues for developing axonal pathways in the telencephalon. *Prog. Mol. Subcell. Biol.* **32**, 1–32 (2003).
66. S. Kondo, H. Al-Hasani, A. Hoerder-Suabedissen, W. Z. Wang, Z. Molnár, Secretory function in subplate neurons during cortical development. *Front. Neurosci.* **9**, 100 (2015).

67. L. Zhuo *et al*., hGFAP-cre transgenic mice for manipulation of glial and neuronal function in vivo. *Genesis* **31**, 85–94 (2001).
68. R. F. Hevner, E. Miyashita-Lin, J. L. Rubenstein, Cortical and thalamic axon pathfinding defects in Tbr1, Gbx2, and Pax6 mutant mice: Evidence that cortical and thalamic axons interact and guide each other. *J. Comp. Neurol.* **447**, 8–17 (2002).
69. E.-M. Amaniti *et al*., Expansion of the piriform cortex contributes to corticothalamic pathfinding defects in Gli3 conditional mutants. *Cereb. Cortex* **25**, 460–471 (2015).
70. J. J. Chun, M. J. Nakamura, C. J. Shatz, Transient cells of the developing mammalian telencephalon are peptide-immunoreactive neurons. *Nature* **325**, 617–620 (1987).
71. A. Antonini, C. J. Shatz, Relation between putative transmitter phenotypes and connectivity of subplate neurons during cerebral cortical development. *Eur. J. Neurosci.* **2**, 744–761 (1990).
72. L. C. deAzevedo, C. Hedin-Pereira, R. Lent, Callosal neurons in the cingulate cortical plate and subplate of human fetuses. *J. Comp. Neurol.* **386**, 60–70 (1997).
73. H. S. Ozaki, D. Wahlsten, Timing and origin of the first cortical axons to project through the corpus callosum and the subsequent emergence of callosal projection cells in mouse. *J. Comp. Neurol.* **400**, 197–206 (1998).
74. S. E. Koester, D. D. O'Leary, Axons of early generated neurons in cingulate cortex pioneer the corpus callosum. *J. Neurosci.* **14**, 6608–6620 (1994).
75. C. Benadiba *et al*., The ciliogenic transcription factor RFX3 regulates early midline distribution of guidepost neurons required for corpus callosum development. *PLoS Genet.* **8**, e1002606 (2012).
76. K. M. Smith *et al*., Midline radial glia translocation and corpus callosum formation require FGF signaling. *Nat. Neurosci.* **9**, 787–797 (2006).
77. L. K. Paul *et al*., Agenesis of the corpus callosum: Genetic, developmental and functional aspects of connectivity. *Nat. Rev. Neurosci.* **8**, 287–299 (2007).
78. A. Hoerder-Suabedissen *et al*., Subset of cortical layer 6b neurons selectively innervates higher order thalamic nuclei in mice. *Cereb. Cortex* **28**, 1882–1897 (2018).
79. S. J. Sanders *et al*.; Autism Sequencing Consortium, Insights into autism spectrum disorder genomic architecture and biology from 71 risk loci. *Neuron* **87**, 1215–1233 (2015).
80. S. De Rubeis *et al*.; DDD Study; Homozygosity Mapping Collaborative for Autism; UK10K Consortium, Synaptic, transcriptional and chromatin genes disrupted in autism. *Nature* **515**, 209–215 (2014).